Understanding Nature's residual strain engineering at the human dentine-enamel junction interface

Tan Sui[1], Alexander J.G. Lunt[1], Nikolaos Baimpas[1,2], Michael A. Sandholzer[3,4], Tao Li[5,6], Kaiyang Zeng[5], Gabriel Landini[3], Alexander M. Korsunsky[1]

[1] Multi-Beam Laboratory for Engineering Microscopy (MBLEM), Department of Engineering Science, University of Oxford, Parks Road, Oxford OX1 3PJ, U.K.

[2] Current address: Atkins Consulting, Trent House, RTC Business Park, London Road, Derby DE24 8UP, U.K.

[3] School of Dentistry, College of Medical and Dental Sciences, University of Birmingham, St Chad's Queensway, Birmingham B4 6NN, U.K.

[4] Institute of Experimental Genetics, Helmholtz Zentrum München, German Research Centre for Environmental Health (GmbH), Ingolstädter Landstrasse 1, 85764 Neuherberg, Germany

[5] Department of Mechanical Engineering, National University of Singapore, Singapore, 117576

[6] Current address: Department of Physics and Astronomy, University of Nebraska-Lincoln, 1400 R St, Lincoln, NE 68588, U.S.

Corresponding author:
Tan Sui

Department of Engineering Science
University of Oxford
Parks Road
Oxford OX1 3PJ
United Kingdom

Tel: +44-18652-83447
Fax: +44-18652-73010

E-Mail: tan.sui@eng.ox.ac.uk

Abstract

Human dental tissue is a hydrated biological mineral composite. In terms of volume and mass, a human tooth mainly consists of dentine and enamel. Human dental tissues have a hierarchical structure and versatile mechanical properties. The dentine enamel junction (DEJ) is an important biological interface that provides a durable bond between enamel and dentine that is a life-long success story: while intact and free from disease, this interface does not fail despite the harsh thermo-mechanical loading in the oral cavity. The underlying reasons for such remarkable strength and durability are still not fully clear from the structural and mechanical perspectives. One possibility is that, in an example of residual stress engineering, evolution has led to the formation of a layer of inelastic strain adjacent to the DEJ during odontogenesis (tooth formation). However, due to significant experimental and interpretational challenges, no meaningful quantification of residual stress in the vicinity of the DEJ at the appropriate spatial resolution has been reported to date. In this study, we applied a recently developed flexible and versatile method for measuring the residual elastic strain at (sub)micron-scale utilizing focused ion beam (FIB) milling with digital image correlation (DIC). We report the results that span the transition from human dentine to enamel, and incorporate the material lying at and in the vicinity of the DEJ. The capability of observing the association between internal architecture and the residual elastic strain state at the micrometre scale is useful for understanding the remarkable performance of the DEJ and may help the creation of improved biomimetic materials for clinical and engineering applications.

Keywords: human dental tissue; dentine-enamel junction (DEJ); residual elastic strain; FIB-DIC

Graphical abstract

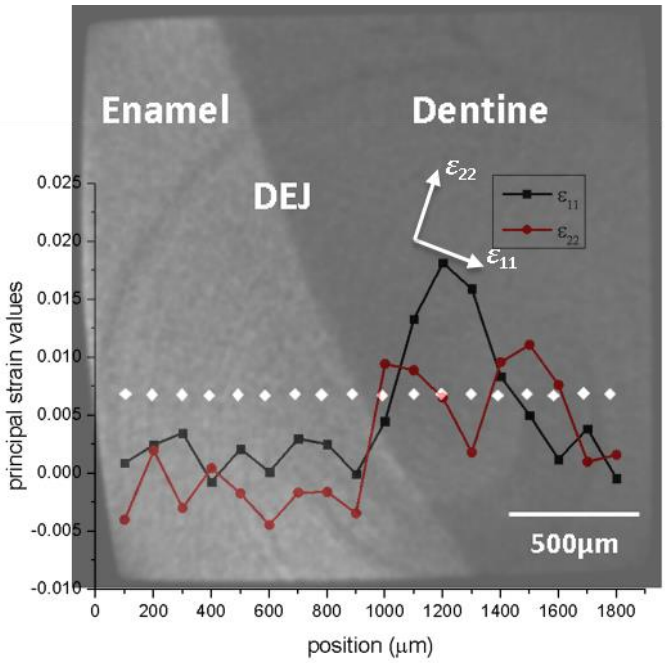

1. Introduction

Human hard dental tissues are nano-structured hierarchical materials combining organic and mineral phases (hydroxyapatite (HAp) crystals) in an intricate and ingenious way to produce remarkable combinations of mechanical strength, chemical stability, wear resistance and thermal endurance. The knowledge of the microstructural features of dental tissues (enamel, dentine and their junction) is important in order to understand their natural properties, and the mechanisms that contribute to their life-long success during mastication, as well as the prediction of the factors that affect the performance of tissues in disease, treatment, environmental and thermal exposure.

Dentine and enamel differ in terms of volume fraction of mineral (50% in dentine and 80-90% in enamel), crystal size and shape of HAp crystals as well as crystal perfection [1-5]. They are joined by an important internal interface, the dentine-enamel junction (DEJ). It has three-level structure [6] consisting of macro-scalloping (wavy

shape) that extends over tens of microns (up to 100 μm), micro-scalloping that covers the range of a few microns, and finally the sharper sub-micron enamel-dentine interface that can be perceived at nano-scale resolution. The band that corresponds to the DEJ and in which the structure and function of tissue undergoes gradual transition can span up to ~200 μm overall in width on the dentine side. This band accommodates the property variation between enamel and dentine by undergoing greater amount of deformation compared to central coronal dentin [7]. Unless diseased, this interface never fails, despite the extreme thermo-mechanical loading it is subjected to in the oral cavity. This stands in stark contrast to the interfaces achieved between artificial dental restorative materials and dentine [8]. The DEJ thus constitutes an excellent example on how to engineer a strong, durable bond between remarkably dissimilar materials: the hard and stiff brittle enamel, and the softer, more compliant, but tougher dentine. It is the desire to learn from nature's architecture of mineral-organic composite, hierarchically structured, property gradient materials that provides the motivation for our study.

X-ray diffraction (XRD) is one of the most versatile, powerful methods of structural characterisation and stress evaluation in materials science. However, the applicability of the XRD method of stress evaluation is largely limited to crystalline materials. Furthermore, the internal mechanical interaction within the mineral-organic composite that is the human dental tissue system may not be easily characterised using this approach, since scattering from the denser mineral component dominates strongly over the less dense organic components. Whether the lattice parameter changes of HAp crystallites observed during odontogenesis are due to chemical or mechanical effects remains the subject of much debate. For these reasons, reliable quantification of the residual stresses associated with the DEJ has not yet been achieved.

One recently developed method, the semi-destructive focused ion beam (FIB) milling and digital image correlation (DIC) analysis, can be applied to both crystalline and amorphous materials and to the evaluation of the overall (composite) residual elastic strain. In combination with FIB serial sectioning this allows understanding the internal architecture of materials at the nano-scale. FIB provides a means of small material layer removal at the rate of ~25nm per step with minimal disturbance. This opens up a family of residual stress evaluation techniques that rely on strain relief measurement [9]. A particular flavour of the (sub)micro-scale strain relief methodology is offered by the ring-core milling proposed by Korsunsky et al. [9]. This new methodology has been applied only recently to the study of metallic samples, such as TiN/Au coating on WC-Co substrate, thin films and other materials [10]. Using this approach, short range (a few microns spatial resolution) and long range (fractions of a mm spatial resolution) stress profiles have been successfully determined in a range of engineering materials. However, none of these studies have been performed on human dental tissues, where the particularities of the mineral-organic composite require the application of bespoke FIB milling strategies. Whilst FIB-assisted measurement of microscale mechanical properties (flexural strength, elastic modulus) has been carried out for human dental tissues [11], the effect of residual strain and measurement of it at the appropriate scales has not been reported to the same extent. It is worth noting that the presence of residual strain affects mechanical property measurement and influences tissue strength and durability.

In this study we utilise the observation of strain relief caused by incremental FIB milling to gain an insight into the built-in residual stresses at the human DEJ, and combine it with the high resolution *in situ* scanning electron microscopy (SEM) and X-ray scattering analysis to reveal the mechanisms responsible for delivering structural

integrity at this important natural interface. To our knowledge, this is the first time this type of analysis has been applied to human dental tissues. The work reported here improves our understanding of the performance dental tissues and the complex internal stress state. The knowledge of the architecture and properties of the natural DEJ will benefit the biomimetic engineering of superior dental restorations and prosthetics, and the development of novel materials to emulate the DEJ.

2. Materials and methods

2.1. Sample preparation

In this study, a human third molar freshly extracted with no dental restorations, caries or damage was used for this study (ethical approval obtained from the National Research Ethics Committee; NHS-REC reference 14/EM/112, Consortium reference BCHCDent332.1531.TB). A low speed diamond saw (Isomet Buehler Ltd., Lake Bluff, Illinois, USA) was used to cut a two millimetre thick disk incorporating dentine, enamel and the DEJ of the tooth. A series of polishing papers were used to obtain the final sample in the form of a $2 \times 2 \times 2$ mm^3 cube. A micro-CT scan was carried out (Bruker SkyScan 1172, SkyScan, Kontich, Belgium) and the 3D micro-scale geometry reconstructed using the SkyScan NRECON package to visualise the region of interest as shown in Fig. 1a. The analysis of cross-sectional images allowed identifying the DEJ as an almost linear interface running at ~66^o with respect to the negative direction of the *x*-axis.

2.2. Implementation of the FIB/SEM procedure

In order to eliminate the charging effects on the non-conducting sample during the electron image acquisition, the cuboidal human tooth sample was attached to the SEM stub using silver paint and coated with 10nm thin film of Au in vacuum at 10mA for 90 seconds using a mini sputter coater (SC7620, Quorum Technologies). The increased image contrast from the fine Au nano-particles benefits the digital-image-correlation (DIC) analysis used here for strain evaluation.

Micro-ring core FIB milling was performed using beam voltage of 15 kV with the current of 49 pA, beam size of 50nm, using LYRA3 XM (Tescan-UK Ltd.) instrument in the Multi-Beam Laboratory for Engineering Microscopy (MBLEM) located in the Department of Engineering Science, University of Oxford. High-resolution Scanning Electron Microscopy (SEM) imaging (5×5 nm pixel size) was used to capture a sequence of images during incremental drilling after tilt image correction (Fig. 1b) that accounts for the ion beam column being mounted at the 55^{o} tilt with respect to the electron beam column used for imaging. For each ring-core milling, different milling rates were obtained by calibration for dentine (1.98×10^{-10} μm^3/nA/s) and enamel (3.0×10^{-10} μm^3/nA/s) respectively. Each milling step was set at a nominal value of 50 nm, the inner diameter of the central micro-pillar or "island" was set at 4 μm, and the width of the annular trench was 0.5 μm (Fig. 1d). This geometry provides a balance between strain and spatial resolutions, and provides sufficient surface area to produce reliable estimates of the strain relief. Ten images were captured at each milling step to allow averaging as a means of noise reduction. Overall, 340 images were collected for 34 milling steps for each marker, which took around 30 min per point. The combination of fast milling and imaging in the absence of external sample loading and stable temperature inside the SEM chamber ensures the creep effect is negligible. In contrast, creep is of great importance in the study of dental tissue indentation, e.g. as reported in

[12]. In the present investigation of residual strains, eighteen ring-core milling markers were placed out across the central part of the top surface of the cuboidal tooth sample (9 in the dentine and 9 in the enamel region) with a spacing between milling islands of 100 μm along the *x* direction (Fig. 1c). A semi-automated routine was developed and applied for multiple ring-core millings.

2.3. Digital image correlation (DIC) analysis and profile fitting

Ten images were firstly averaged at each milling step using ImageJ software [13]. DIC analysis on the central micro-pillar surface was conducted using Matlab® code developed by Christoph Eberl [14]. This creates a grid of markers in the region of interest within the image sequence (see Fig. 2a). The relative displacements of the grid of markers with respect to the undisturbed state against pixel position were then fitted with a straight line to determine the displacement gradient, thus obtaining the average strain as a function of image number that corresponds to the consecutive cutting depths, as shown in Fig. 2b. The process of fitting gives rise to a significant number of outliers, i.e. data points that show unusually high or low values that deviate far from the general trend. These points arise as a consequence of inherent noise that arises in the course of image acquisition. In accordance with the well-established procedures for experimental data treatment, outliers were removed prior to further analysis [15]. Manual and automated outlier removal was carried out based on the quality of DIC fitting, ensuring that only well-tracked markers were included in the analysis. Outlier removal was performed based on correlation coefficient thresholding and automated tracking of marker movement relative to each other [16]. Consistent procedures were followed for dentine and enamel.

The above strain evaluation approach quantifies the strain evolution along a single direction in each instance of analysis. To characterise the full residual in plane stress/strain field at each location, the direction of principal stress/strain needs to be determined, which requires at least three strain measurements along different directions. DIC analysis was therefore applied to the original images to determine the strain components in the horizontal (0^o) and vertical (90^o) directions. Further, the images were rotated by 45^o using ImageJ software [13], and DIC analysis was applied in the new horizontal and vertical directions to calculate the strain components at 45^o and 135^o in the original images. The standard deviation of the linear fitting process was calculated for each image. The inverse of this value was used as a measure of the goodness of fit for each strain value. These values were used as weighting inputs for the strain profile fitting. In sum, strain components along four directions 0^o, 45^o, 90^o and 135^o were calculated, as illustrated in Fig. 1c. This approach also allows evaluating the robustness of analysis by comparing the calculated principal strain components and directions by different combinations of measurements along selected three directions.

Korsunsky et al. [17] proposed a master function curve to describe the general relationship between the relative milling depth in the micro-pillar milling method, and the observed strain relief,

$$f(\Delta\varepsilon_\infty, z) = 1.12\Delta\varepsilon_\infty \times \frac{z}{(1+z)}\left[1 + \frac{2}{(1+z^2)}\right] \quad (1)$$

where $z = (h/0.42d - \delta_{start})$, h is the cut depth, d is the ring core diameter, $\Delta\varepsilon_\infty$ is the strain at full relief (at infinite cut depth) and δ_{start} represents the zero-depth offset parameter that accounts for surface position uncertainty due to roughness. After obtaining the profiles of strain against image number using DIC, least-squares fitting was used using the master function (Fig. 2 c&d) to determine the full strain relief in

each micro-pillar in the 18 implementations of FIB-DIC ring-core milling. Thus, the profile of principal strain value and orientation variation from dentine to enamel across the DEJ was obtained.

In summary, after the image collection and pre-processing including image averaging and image rotation, the key steps in the DIC processing and residual elastic strain determination were as follows:

- DIC analysis: introduction of markers defining local tracking points within the stub region (Fig. 2a), determination of their displacements and outlier removal, followed by line fitting to extract the strain value equal to the line slope (Fig. 2b)
- Strain depth profile fitting: Least squares fitting of DIC strain profile predicted by the master function (green line in Fig. 2c &d) to obtain the complete strain relief value.
- Residual elastic strain evaluation: This value is equal in magnitude and opposite in sign to the complete strain relief. The principal strain value is then calculated from regression analysis of the four strain components.

3. Results

The calculated residual elastic strain profiles from FIB-DIC along the four different directions are plotted in Fig. 3, represented by the solid black (0^o), red (45^o), blue (90^o) and pink (135^o) curves, respectively. The enamel covers the region from 0-900 μm in terms of the measurement position, and dentine lies in the range of 900-1800 μm.

The first observation that needs to be made in order to place the results in context is that material removal techniques, such as the FIB-DIC micro-ring-core method used here, measure the *overall*, i.e. composite residual elastic strain that arises from the

combination of contributions from the constituents (in the present study these are HAp crystallites and the organic matrix).

Further general observations on the four strain profiles reveal that the average absolute value of the residual elastic strain in enamel is much smaller than in dentine, as may be expected due to its significantly higher stiffness. Overall, tensile residual stress is present in dentine. In contrast, although the residual elastic strain value in the enamel is close to zero (lying within the error bar bound), it is hard to identify the sign of residual strain/stress in enamel from the data, although from considerations of balance residual compression is expected. In addition, the residual elastic strain value in the enamel is found to be approximately uniform, with a sharp transition observed in the region 900-1000 μm, i.e. approaching to the DEJ, where the residual elastic strain value changes dramatically. Further beyond this position into the dentine region, a steep variation of the residual elastic strain is observed, although the average value remains almost the same, followed by a drop to near zero when the free edge of the sample is approached at 1800 μm. The zero residual elastic strain at both edges is attributed to the traction-free surface effect. The steep gradient around the DEJ is associated with local microstructural and built-in residual stress variation that is discussed in detail below.

To understand the details of the residual elastic strain state in this system, the full four strain components (0^o, 45^o, 135^o and 90^o) were used to calculate the principal strain values (ε_{11}, ε_{22}), as shown in Fig. 4a. A similar trend was observed to that shown in Fig. 3, where small values of principal strains are observed in the enamel, whilst in the dentine steep changes are seen near the DEJ. At the DEJ the two principal strains are of similar magnitude, indicating an approximately equi-biaxial strain state. However, they differ significantly within the range of about 400 μm beneath the DEJ (positions

1000-1400 μm), and then decay towards the edge, as highlighted by the grey rectangle. The principal strain directions were also calculated for all the measurements and are shown in Fig. 4b. Since the sign and orientation of the principal strains in enamel is difficult to quantify due to the smallness of values in comparison with the error bars, we focus our attention on the results for dentine, in the region where the determination of principal strain orientation is meaningful due to the significant difference between principal values, in the region of interest beneath the DEJ at 1000-1400 μm positions. From the three measurement points at 1100 μm, 1200 μm and 1300 μm, the average principal direction orientation is 25°, and the direction of the principal strain component ε_{11} shown in Fig. 4c by the red arrow points at 25° clockwise from horizontal direction at 0°.

4. Discussion

4.1. Failure and the residual elastic strain variation

The measurement of the residual elastic strain (Fig. 3) and the two principal strain values (Fig. 4a) in dentine imply tensile pre-existing intrinsic residual stress. In terms of stress equilibrium in the bulk, a compressive intrinsic residual stress field must pre-exist in enamel. This residual stress state in the vicinity of the human DEJ is likely to provide a built-in mechanism for strength improvement and failure avoidance under the loads experienced by human teeth. The compressive residual stress in the brittle enamel ensures that under unevenly distributed contact pressure loading that may occur during mastication of hard substances in diet, local stresses remain compressive throughout. The tensile residual stress field can be readily accommodated by the more ductile and tough dentine that contains large volume fraction (up to 50%) of organic constituents that are exceptionally good at accommodating large strains without failure. This is

particularly true in shear that may allow ‘slip-and-stick’ deformation, with internal bonds being released and re-made, retaining tissue integrity [5]. Furthermore, for the region lying beneath the DEJ in dentine, where the largest non-equi-biaxial residual elastic strain is found, a correlation can be established with the local ultrastructure, as discussed in the next section.

4.2. The relationship between residual elastic strain variation and hierarchical structure

The difference in the stiffness and the consequent observation of the different residual elastic strain values in dentine and enamel arises as a consequence of the structural and compositional differences between the two materials at the micro- and nano-scales. Both dentine and enamel can be regarded as two-level hierarchical composites [18, 19], as illustrated here using atomic force microscopy (AFM) images with 4×4 nm pixel size in Fig. 5. At the larger, micro-level, the structure of enamel consists of aligned key-hole shaped rods within a composite matrix (Fig. 5a), whilst that of dentine is characterized by a numerous aligned hollow tubules (Fig. 5b). At the second, nano-level, the material can be thought as the matrix identified at the larger structural level (intertubular and peritubular dentine, and the rod material in the enamel), which itself is of a composite nature, consisting of partially aligned hydroxyapatite (HAp) crystallites (hard component) embedded in an organic matrix (soft component) (Fig. 5c and d). The structural differences between dentine and enamel are manifested, to some extent, in the volume fraction and morphology of the hard and soft constituents at different scales, causing differences in their stiffness, hardness and brittleness. The observed steep transition in the residual elastic strain in the vicinity of the DEJ built

into the structure optimizes the mechanical performance of dentine in the vicinity of the interface with the much harder, highly mineralized enamel [18, 19].

To understand the mechanisms of residual elastic strain generation and deformation accommodation, we compare the residual elastic strain profiles in Fig. 3 and the principal strain profiles in Fig. 4a with the degree of alignment of HAp crystallites (percentage of aligned particles) measured and reported previously for these systems by small-angle X-ray scattering technique [20, 21]. The highest degree of alignment occurs at about 100-200 μm beneath the DEJ in the dentine, as shown in Figs. 4d & e. This coincides with the location of the maximum absolute value of residual elastic strain shown in Fig. 3 and principal strain values in Fig. 4a, i.e. the position of the highest residual stress. The major (most positive) principal strain direction (ε_{11}) lies perpendicular to the preferred orientation (*c*-axis) of HAp crystals at this area, as shown in Fig. 4d. This indicates that the residual stress is mostly tensile along the preferred orientation of HAp crystals. This is consistent with the anisotropic stiffness of HAp crystals in dentine, with the preferred orientation of crystallites also being the stiffest direction. The high degree of alignment of HAp crystallites beneath the DEJ provides an important mechanism for the transfer and redistribution of mastication and thermal loads from enamel into dentine. When external loading or temperature change give rise to a local compressive stress in the near-DEJ region, the anisotropic nature of the local composite material stiffness means that it is mostly taken up by the stiff direction aligned with the *c*-axis of the crystallites. The pre-existing tensile residual stress in this direction mitigates this compression. When, on the other hand, the external load application causes additional tension, this decreases the difference between the principal stresses along and perpendicular to the preferred orientation direction of

crystallite (which is equal to twice the shear stress on the corresponding plane), reducing the propensity for plastic deformation.

Compared with the identified region of interest beneath the DEJ, the effect of preferred orientations at other regions is low, with a lower degree of alignment indicating that the distribution of HAp crystals becomes close to random. Concomitantly, near equi-biaxial residual elastic strain state is observed in these regions.

4.3. Potential origins of residual elastic strain near the DEJ

The origin of the residual elastic strain near the DEJ may be pre-existing stress concentration that is incorporated into the system during the formation of dental tissues (dentinogenesis and amelogenesis) occurring outwards from the DEJ towards dentine and enamel [22]. Evidence has shown that the initial mineralization occurs in small nuclei near the DEJ within supramolecular aggregates of amelogenins and enamelins. Soon thereafter, the HAp crystallites become confluent with the smaller hydroxyapatite crystallites in the neighbouring dentine [23]. As a general comment, since a tooth in its lifetime undergoes frequent cyclic loading during mastication, much of the load on the teeth is being transmitted from the occlusal surface through the rather thin outer layer of enamel that is more resistant to compression than the inner dental tissues to the dentine that are protected by the built-in residual stress system. As a result, stress is most likely to concentrate and is stored in the DEJ, which could not be fully relieved by the sample cutting.

4.4. Sample dehydration effect

The high vacuum present within the scanning electron microscope chamber may induce dehydration of the samples during experimentation. Although no systematic

study one the effects of vacuum has been reported for dentine, a careful investigation was carried out for bone, which has structure and properties very close to those of dentine [24]. The authors showed that placing samples in vacuum did not induce significant dehydration or modification of the mechanical bone properties. Therefore, it should be concluded that the environment of the SEM vacuum chamber does not affect the sample state to any significant extent over the duration of FIB ring-core milling. Hence, the residual strain measured by FIB-DIC ring-core method corresponds to the inherent strain state within the sample and is not affected by the possibility of dehydration. We also noted that since enamel has much higher mineral and much lower organic content, any effect of vacuum is likely to be significantly weaker than in dentine, suggesting that our results are representative of the real state of the tooth.

4.5. Residual elastic strain measurement by the FIB-DIC method

A number of interrelated parameters need to be taken into consideration when the FIB-DIC method is applied to different samples. i) Sample conductivity: a few nanometers layer of coating are needed for the non-conductive sample to reduce the imaging charging, but this should not to introduce any significant stress. Meanwhile, the improved image contrast brought by the coating layer also facilitates the DIC analysis; ii) Stub (island) diameter: smaller stub diameters result in an improved spatial resolution for stress mapping, but at the same time the final surface area for the analysis is reduced, potentially giving rise to greater uncertainties. Since this region is used to quantify the strain through DIC, it can therefore result in erroneous overestimation of the calculated stress value. iii) Ring core width: a trench width wide enough to ensure relaxation of the central stub is required. However, very wide trench widths may result in large amounts of re-deposition of cut material onto the DIC surface. iv) Milling

setting: a higher milling rate results in images with higher signal-to-noise ratio and increased re-deposition. However, faster milling rates reduce imaging damage and minimise the effect of beam drift. Furthermore, the higher currents and voltages result in improved trench profiles, but these also increase the inference between the ion and electron beams as well as the effects of surface charging.

As shown in Fig. 3, the errors associated the result along 90^o direction (indicated by the blue markers) were larger than those along other directions. One possible reason for the non-equal errors along the two directions may be the arrangement of FIB/SEM in the chamber (illustrated in Fig. 1b). Since the electron imaging is performed by horizontal scanning, i.e., along *x*-axis, even slight shifts in position between incremental vertical scan positions (90^o) can result in potentially higher levels of noise than the horizontal direction (0^o). Another possible reason for the uneven error bar lengths is associated with image contrast differences along different directions, and from the underlying dental tissue anisotropy that affects the quality of DIC marker tracking.

Since human dentine contains a significant volume fraction of organic material, the possibility of time-dependent response to stress relief due to milling must be considered. X-ray scattering studies of time-dependent deformation of dentine [25] reveal that creep-induced strains during the first 30 minutes (that correspond to the duration of the FIB milling and SEM imaging operation) are negligible. In other words, the strain relief perceived at the surface of the micro-pillar corresponds to the instantaneous part of sample deformation response.

To evaluate the possibility of SEM imaging causing sample surface modification that affects the strain measurement, repeated imaging was carried out, and the level of noise evaluated. It was found to be of the order of 10^{-4}, i.e. significantly lower than the strains measured and reported in this study.

4.6. Statistical analysis

In this section we discuss the statistical aspect of the results reported in this study. Careful statistical analysis was performed throughout the study to assess the significance of results, and equip the reported values with error estimates. As this is the first report of residual strain evaluation in human dental tissues at the micron scale using FIB-DIC ring-core, it was not possible to carry out direct comparison with other samples drawn from other study groups. Furthermore, since samples for our studies are drawn from the anonymised Human Dental Tissue Bank, no attribution in terms of gender, race or age was possible. However, it is appropriate to refer to our supporting investigations using synchrotron X-ray scattering and imaging that show broad consistency across the range of dozens of samples in terms of crystal and nanoscale structure, and such residual strain indicators as the lattice parameter of HAp crystallites. The present study provides a much needed link between these indirect measures of residual strain that depend on the reference unstrained lattice parameter d_0, and absolute measures of residual strain obtained by FIB-DIC ring-core milling.

Statistical support for error evaluation was provided using the analytical approach reported in [16]. Error bars were given for all experimental data points, accompanied by explanations in the text. Typical error of strain evaluation in dentine and enamel by FIB-DIC ring-core milling was found to be of the order of 5×10^{-3}.

5. Conclusions

In this study, the novel semi-destructive FIB-DIC methodology has been applied the first time to human dental tissue, to achieve sub-micron resolution in the elastic residual elastic strain measurement. The variation of the residual elastic strain across the dentine,

DEJ and enamel showed a large elastic residual strain observed in dentine compared with that in enamel. The examination of the residual elastic strain across the junction can also be used to reveal the complex residual stress state in the vicinity of the DEJ. Moreover, the principal strain direction and values determined by the calculation of multiple strain components indicates that it is associated with the orientation of the DEJ.

Through this novel experimental work, we are able to observe the internal architecture of human dental tissues and their mechanical behaviour at the nano-scale. Understanding residual stress has significant clinical relevance in improving our knowledge of the architecture and properties of the natural DEJ, and will further benefit biomimetic design and clarify how residual stress contributes to the remarkable durability of dental materials, both natural and artificial.

Acknowledgements

AMK acknowledges funding received for the MBLEM laboratory at Oxford through EU FP7 project iSTRESS (604646), and access to the facilities at the Research Complex at Harwell (RCaH), under the Centre for In situ Processing Studies (CIPS). The authors have declared no conflict of interest.

References

[1] De Sant'anna GR, Dos Santos EAP, Soares LES, Santo AMD, Martin AA, Duarte DA, et al. Dental Enamel Irradiated with Infrared Diode Laser and Photoabsorbing Cream: Part 1-FT-Raman Study. Photomed Laser Surg 2009;27:499-507.

[2] Vennat E, Bogicevic C, Fleureau JM, Degrange M. Demineralized dentin 3D porosity and pore size distribution using mercury porosimetry. Dent Mater 2009;25:729-35.

[3] Johansen E, Parks HF. Electron Microscopic Observations on the 3-Dimensional Morphology of Apatite Crystallites of Human Dentine and Bone. J Biophys Biochem Cy 1960;7:743-&.

[4] Voegel JC, Frank RM. Ultrastructural-Study of Apatite Crystal Dissolution in Human Dentin and Bone. J Biol Buccale 1977;5:181-94.
[5] Gao HJ, Ji BH, Jager IL, Arzt E, Fratzl P. Materials become insensitive to flaws at nanoscale: Lessons from nature. P Natl Acad Sci USA 2003;100:5597-600.
[6] Marshall SJ, Balooch M, Habelitz S, Balooch G, Gallagher R, Marshall GW. The dentin-enamel junction - a natural, multilevel interface. J Eur Ceram Soc 2003;23:2897-904.
[7] Milicich G, Rainey JT. Clinical presentations of stress distribution in teeth and the significance in operative dentistry. Pract Periodontics Aesthet Dent 2000;12:695-700; quiz 2.
[8] White SN, Miklus VG, Chang PP, Caputo AA, Fong H, Sarikaya M, et al. Controlled failure mechanisms toughen the dentino-enamel junction zone. J Prosthet Dent 2005;94:330-5.
[9] Korsunsky AM, Sebastiani M, Bemporad E. Focused ion beam ring drilling for residual stress evaluation. Mater Lett 2009;63:1961-3.
[10] Lunt A, Baimpas N, Salvati E, Dolbnya IP, Sui T, Ying S, et al. A state-of-the-art review of micron scale spatially resolved residual stress analysis by ring-core milling and other techniques. Journal of Strain Analysis for Engineering Design 2015;in press.
[11] Chan YL, Ngan AH, King NM. Nano-scale structure and mechanical properties of the human dentine-enamel junction. J Mech Behav Biomed Mater 2011;4:785-95.
[12] Chuang SF, Lin SY, Wei PJ, Han CF, Lin JF, Chang HC. Characterization of the elastic and viscoelastic properties of dentin by a nanoindentation creep test. J Biomech 2015;48:2155-61.
[13] Rasband WS. ImageJ. http://imagejnihgov/ij/. Bethesda, Maryland: U.S. National Institutes of Health; 1997-2014.
[14] Digital Image Correlation (DIC) code di-hatJHU, running in Matlab, free download from, http://www.mathworks.com/matlabcentral/fileexchange/12413.
[15] Rousseeuw P, Leroy A. Robust Regression and Outlier Detection. 3rd ed. ed: John Wiley & Sons; 1996.
[16] Lunt A, Korsunsky AM. A review of micro-scale focused ion beam milling and digital image correlation analysis for residual stress evaluation and error estimation. Surf Coat Tech 2015;In press.
[17] Korsunsky AM, Sebastiani M, Bemporad E. Residual stress evaluation at the micrometer scale: Analysis of thin coatings by FIB milling and digital image correlation. Surf Coat Tech 2010;205:2393-403.
[18] Sui T, Sandholzer MA, Baimpas N, Dolbnya IP, Walmsley AD, Lumley PJ, et al. Multi-scale modelling and diffraction-based characterization of elastic behaviour of human dentine. Acta Biomater 2013;9:7937-47.
[19] Sui T, Lunt AJ, Baimpas N, Sandholzer MA, Hu J, Dolbnya IP, et al. Hierarchical modelling of in situ elastic deformation of human enamel based on photoelastic and diffraction analysis of stresses and strains. Acta Biomater 2014;10:343-54.
[20] Sui T, Sandholzer MA, Le Bourhis E, Baimpas N, Landini G, Korsunsky AM. Structure-mechanical function relations at nano-scale in heat-affected human dental tissue. J Mech Behav Biomed 2014;32:113-24.
[21] Marten A, Fratzl P, Paris O, Zaslansky P. On the mineral in collagen of human crown dentine. Biomaterials 2010;31:5479-90.
[22] Sui T, Ying S, Korsunsky AM, Landini G. X-ray Study of Human Dental Tissues Affected by Erythroblastosis Fetalis. Journal of Dental Research 2015;94:1004-10.

[23] Klionsky DJ, Abdalla FC, Abeliovich H, Abraham RT, Acevedo-Arozena A, Adeli K, et al. Guidelines for the use and interpretation of assays for monitoring autophagy. Autophagy 2012;8:445-544.
[24] Jimenez-Palomar I, Shipov A, Shahar R, Barber AH. Influence of SEM vacuum on bone micromechanics using in situ AFM. J Mech Behav Biomed Mater 2012;5:149-55.
[25] Singhal A, Deymier-Black AC, Almer JD, Dunand DC. Effect of stress and temperature on the micromechanics of creep in highly irradiated bone and dentin. Mat Sci Eng C-Mater 2013;33:1467-75.

Figure captions:

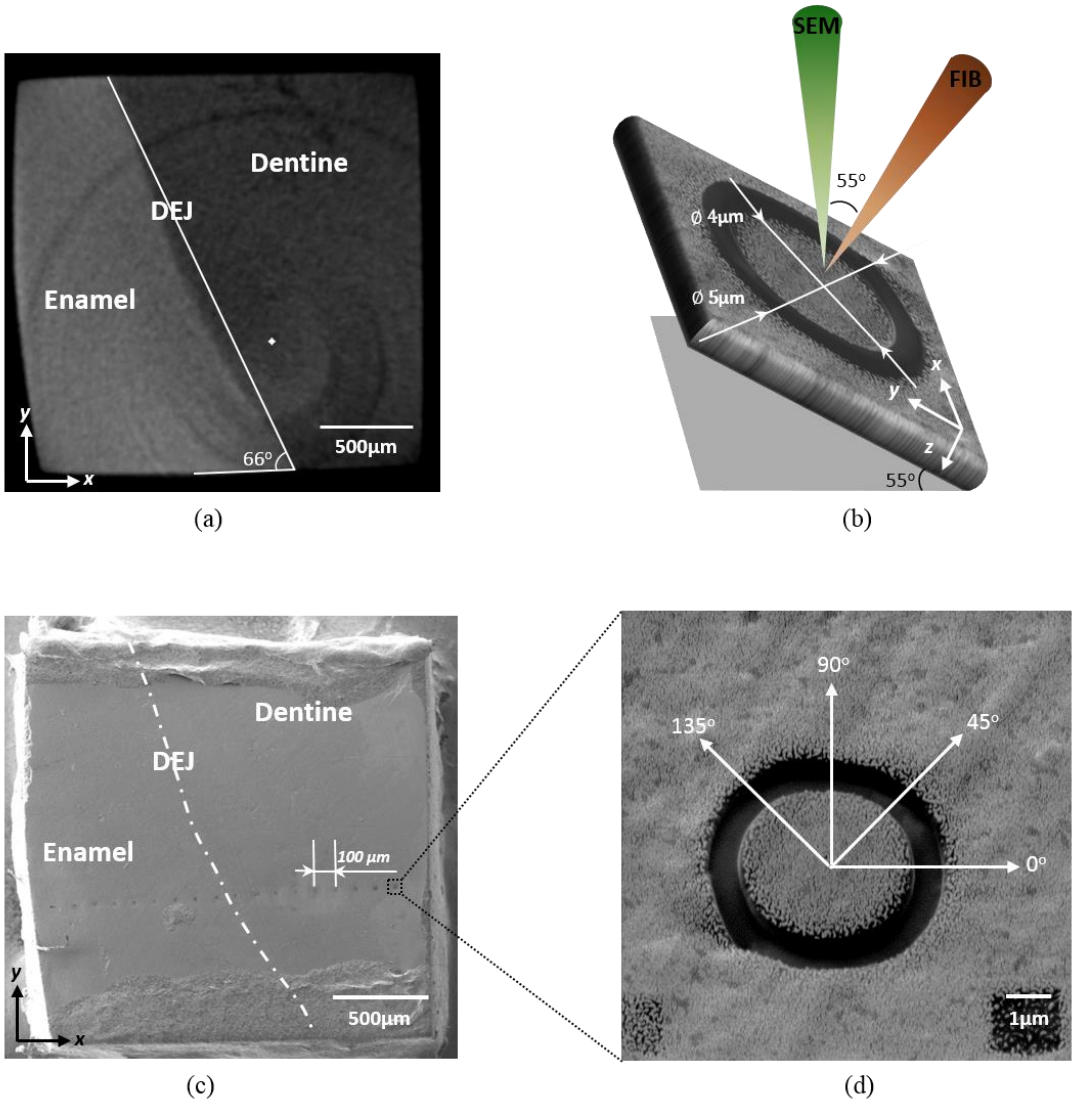

Fig. 1. Illustration of the sample and micro-ring core FIB milling. (a) Micro-CT reconstruction of a cuboidal tooth sample showing absorption contrast between dentine and enamel. (b) Illustration of the semi-automated procedure for ring-core FIB drilling and SEM image acquisition. (c) SEM image of tooth sample presenting the milling positions across the DEJ. (d) A snapshot from the incremental ring-core FIB milling sequence at a single point. White arrows indicate the four strain component evaluation directions.

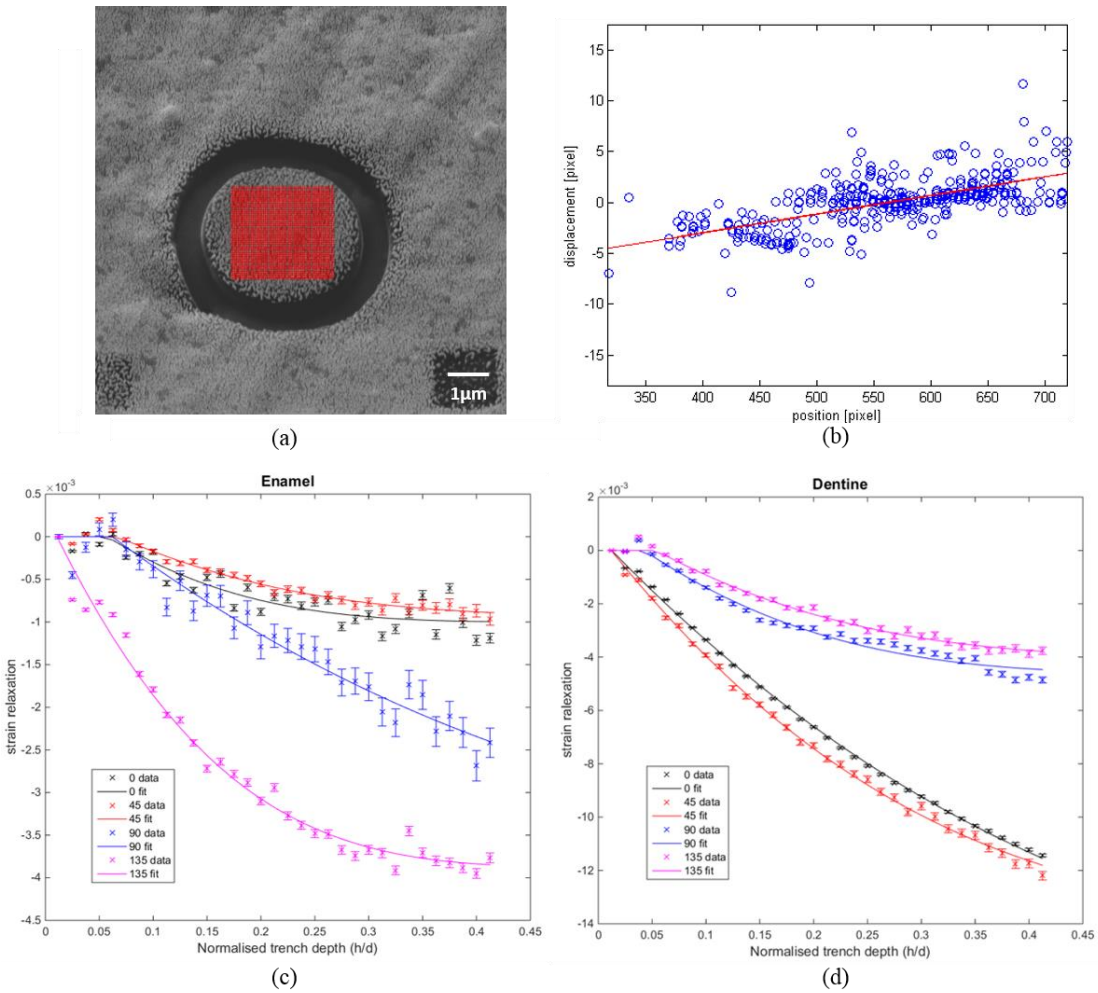

Fig. 2. DIC analysis procedure. (a) Virtual grid of makers at the micro-pillar surface. (b) Automated DIC analysis of displacement vs pixel position, indicating the linear fit. Least-squares fitting of the strain relief master curve to the DIC strain depth profile in (c) enamel and (d) dentine.

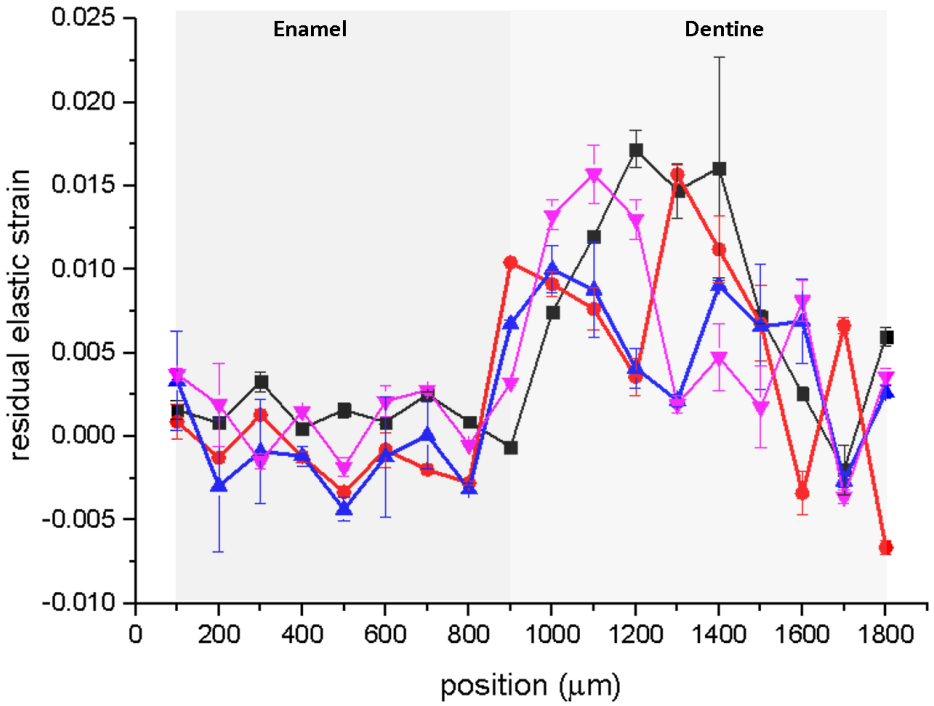

Fig. 3. Residual elastic strain components obtained from FIB-DIC measurements. Four directions 0º (black), 45º (red), 90º (blue) and 135º (pink) were plotted with respect to the position. The range of positions spans the enamel (0-900 μm) and dentine (900-1800 μm), and straddles the DEJ.

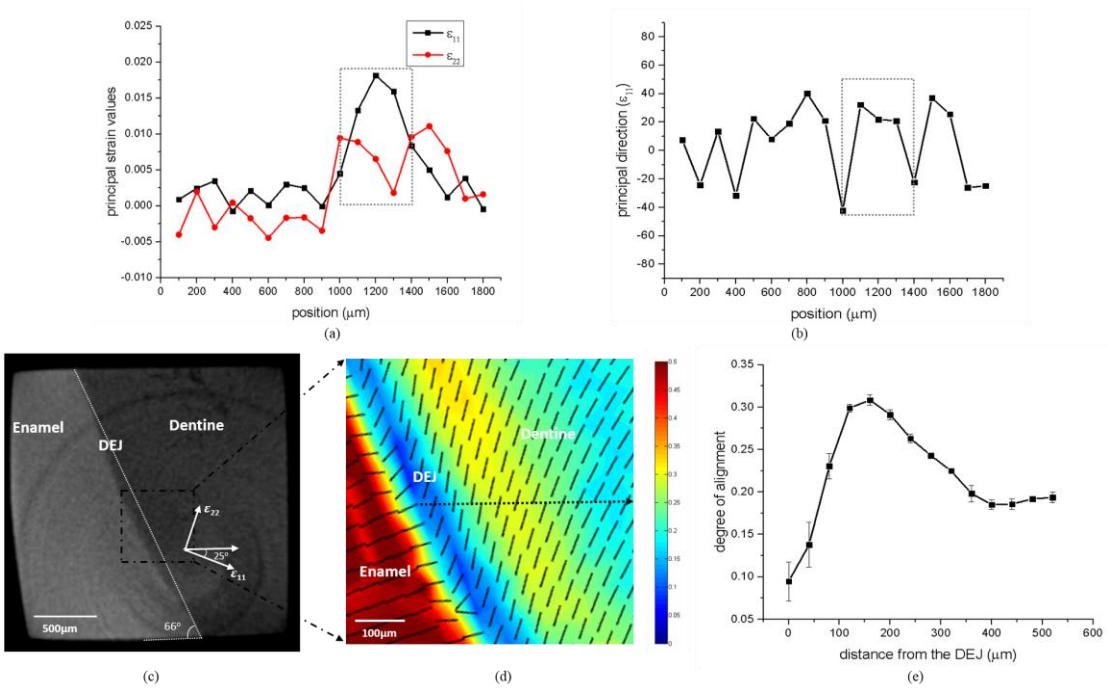

Fig. 4 Principal strain values and principal strain direction. (a) Principal strain values across 18 measurements. (b) Principal strain direction is illustrated in black. (c) Direction of the principal strain component ε_{11} is shown in red line with average value 25º. (d) 2D map of degree of alignment of HAp crystallites, with the crystal orientation marked by the black lines. (e) Degree of alignment of HAp crystallites from the DEJ to dentine.

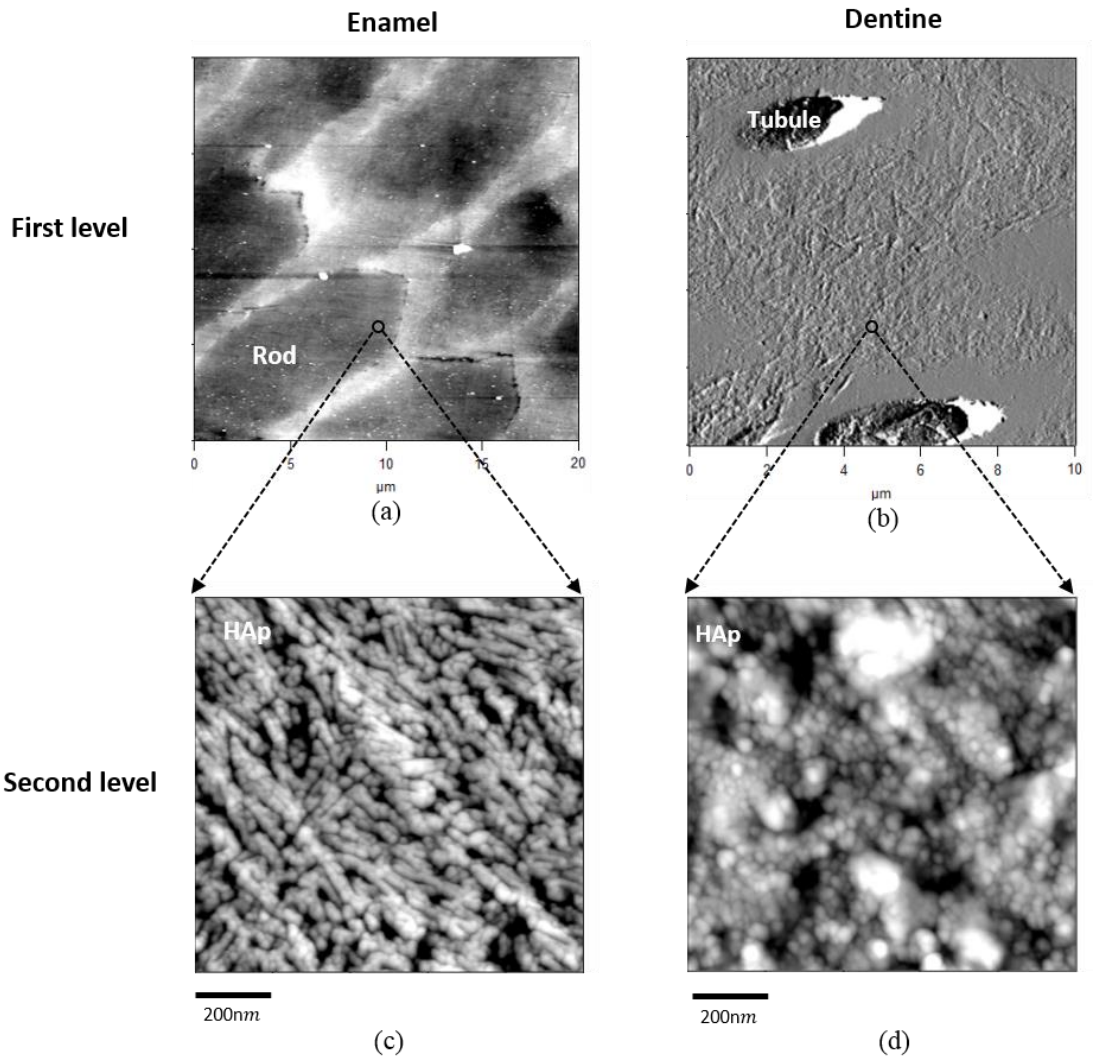

Fig.5. The two-level hierarchical structure of human dental tissues captured by AFM. The micron scale image shows (a) the rod structure in enamel, and (b) tubule structure in dentine. The nano-scale image shows the HAp crystallite morphology and distribution in (c) enamel and (d) dentine.